Summary of the Changes to Reviewer 1's Recommendations and Comments

Journal: Natural Hazards and Earth System Sciences

Ref: NHESS-2024-86

Title: Predicting Deep-Seated Landslide Displacements in Lushan Mountains through the Integration of Convolutional Neural Networks and an Age of Exploration-Inspired Optimizer

The authors appreciate the reviewer's valuable feedback. The summary of the changes based on the reviewer's recommendations & comments is listed below. All the revisions are TRACKED in the re-submitted WORD file along with marked RED COLOR for the ease of the reviewer's perusal. Our colleague, a native English speaker of BLUE COLOR, has corrected grammatical and writing style errors in the original version.

Recommendations and Comments of Reviewer	Authors' Summary of the Changes
This paper by Chou et al. describes an effort to test the sensitivity of various machine learning models on forecasting deep-seated landslide displacement over single-day and weeklong timescales. The authors utilize two sets of extensometer data that record landslide displacement at Lushan Mountain in Taiwan over a period from 2009-2017, along with four records of groundwater well data and satellite-derived temperature and humidity data. Over this time, the extensometer data record multiple pulses of movement that appear to correspond to peaks in groundwater levels, suggesting a connection to pore-water pressure increases via rising water tables. The authors employ their record of time series data to train a bevy of various AI models, and then from the two top-performing models fine-tine their hyperparameters using a newly released optimization algorithm (the Age of Exploration-Inspired Optimizer, or AEIO). The authors find that: 1) many models perform well in forecasting landslide displacement although there are tradeoffs between accuracy and computation time (impressively low errors from ~4-7% in the best cases); and 2) the AEIO algorithm successfully reduces uncertainty in their top models. Overall, the authors present a clear description of the AI models used in the analysis and show convincingly that for the study monitoring sites machine learning algorithms can indeed be used to accurately forecast landslide displacement, even at the multi-day time scale. Showing that these	As authors, we wish to express our sincere gratitude to the reviewers for their time and effort in thoroughly evaluating our research. We are encouraged by the recognition that our study may contribute to NHESS. In response to the reviewers' insightful suggestions, we will revise our manuscript accordingly. The following sections will address each revision in detail. We hope that these updates will meet the reviewers' expectations and align with the high standards of NHESS for publication.

methods yield a ~5% error on a seven-day forecast of landslide displacement is highly impressive and has obvious societal relevance. The AEIO method (complete with a very fanciful Fig. 8) does appear to work well in reducing the prediction uncertainty for the top-performing models. Therefore, I think the paper succeeds in showing the practical utility of applying optimized AI-based methods to this type of extensometer data and the benefits of running an optimization scheme on improving model performance. As presented, however, the manuscript feels somewhat lopsided as there is comparatively little information about the landslide itself and any in-depth analysis on connections from the model(s) to the results. For example, how much does the choice of input parameters impact performance? Are four groundwater datasets necessary, or would one suffice? Does including humidity data actually help improve model results, or is it extraneous? These are the types of questions worth discussing that may help yield more insight and understanding that may expand the utility of these results beyond the authors' study data (and thus would be of increased relevance to the global NHESS readership). Beyond these primary concerns, there are a number of smaller line-by-line technical and editorial comments I provide below that warrant addressing by the authors. If the authors can address these comments, I think this manuscript will make a useful contribution to NHESS.	
1: I'm not sure the phrase "in Mountains" is necessary here. 2: I believe the word "an" should perceive "Age of Exploration-Inspired Optimizer".	We have identified inaccuracies in the title based on the reviewer's comments. We will replace the phrase "in Mountains" with "in Lushan Mountain" to provide readers with more precise information about the data collection and research location. Additionally, as suggested by the reviewer, we will add the word "an" before "Age of Exploration-Inspired Optimizer.". **Predicting Deep-Seated Landslide Displacements in Lushan Mountains through the Integration of Convolutional Neural Networks and an Age of Exploration-Inspired Optimizer** **Jui-Sheng Chou[1,*], Hoang-Minh Nguyen[1], Huy-Phuong Phan[1], Kuo-Lung Wang[2]** [1] Department of Civil and Construction Engineering, National Taiwan University of Science and Technology, Taipei, Taiwan [2] Department of Civil Engineering, National Chi Nan University, Nantou, Taiwan (jschou@mail.ntust.edu.tw; hoangminhkg1992@gmail.com; huyphuong777@gmail.com; klwang@ncnu.edu.tw) *Correspondence e-mail address: jschou@mail.ntust.edu.tw
9: Nothing is done in this manuscript to show that deep-seated landslides are becoming increasingly frequent due to changing climate patterns. Is there a reference the author can provide that shows this in	We greatly appreciate the reviewer's comment. The reviewer correctly pointed out that our study does not demonstrate the argument that deep-seated landslides are becoming more frequent due to

order to justify its presence in the abstract? This is certainly a nuanced topic as projected climatic changes may impact different areas (and thus landslide-triggering potential) differently across the globe, and therefore it is difficult to make these blanket statements. 11: insert “by” after “displacements”	changing climate patterns. As such, it is inappropriate to include this argument in the abstract, and we have revised the sentence accordingly. Additionally, we have added the word "by" after "displacement," as suggested by the reviewer. **Abstract** Deep-seated ~~landslides, becoming increasingly frequent due to changing climate patterns, pose significant risks to human life and infrastructure. This research contributes to~~ Landslides have caused substantial damage to both human life and infrastructure in the past. Developing an early warning system for this type of disaster is crucial to reduce its impact on society. This research contributes to developing predictive early warning systems for deep-seated slope displacements by employing advanced computational models for environmental risk management. Our novel framework integrates machine learning, time series deep
25: There are certainly more than 378 landslides recorded worldwide between 1997 and 2017. Is this a specific subset of slides from this study? If so, a little more context needs to be provided here on what this number represents.	In this section, we aim to provide data to demonstrate that landslides have significant negative impacts on our lives. However, as suggested by the reviewer, it appears that the data used may not be accurate. Therefore, we have sought new data and revised this section accordingly. **1. Introduction** ~~The 378 landslides recorded worldwide between 1997 and 2017 resulted in the deaths of 18,414 people and left 4.8 million others injured, with associated costs estimated at around USD 8 billion (Ageenko et al., 2022)~~ Landslides are among the most devastating natural disasters (Huang and Fan, 2013), claiming an average of over 4,000 lives annually worldwide between 2004 and 2010 (Petley, 2012). Landslides represent a global hazard, particularly in developing countries, where rapid urbanization, population growth, and significant land use changes occur (Caleca et al., 2024). The identification,
35: The 10 m threshold for defining a deep-seated landslide seems arbitrary. Dou et al. (2015) use 10 m as an example in their example sketch (their Fig. 5), but they do not reference this as a specific genetic guideline. Please use a more appropriate definition here.	We fully agree with the reviewer that using the definition of “deep-seated landslide” from Dou et al. (2015) was inappropriate. Consequently, we have revised this paragraph to adopt the definition provided by Lin et al. (2013) and included the relevant references. We hope this revised definition offers greater clarity and accuracy, addressing the reviewer's concerns. al., 2014). These issues are further exacerbated in countries with complex geological and climatic conditions. ~~Deep-seated landslides, or gravitational deformations, involve slow movement of soil or rock at depths greater than 10m, impacting large areas and leading to significant debris flows (Dou et al., 2015)~~. A deep-seated landslide involves the gradual and persistent displacement of a substantial amount of soil and rock, which can escalate into a sudden and devastating event (Kilburn and Petley, 2003; Geertsema et al., 2006; Chigira, 2009). Unlike shallow landslides, which typically affect surface layers to a depth of a few meters, deep-seated landslides extend deeper, often exceeding 10 meters, and can involve the movement of underlying bedrock (Lin et al., 2013). Predicting these events is challenging and costly (Thai Pham et al., 2019). Therefore, extensive efforts have been made to predict such disasters throughout history. One method that has been employed involves thoroughly examining the physical and geological
41-42: This sentence feels out of place here since the paragraph is just discussing background. It would fit better in the final paragraph of this section outlining the goals of the specific study (i.e., lines 63-76)	We agree that the inclusion of this sentence in this paragraph is not appropriate as it only discusses the background of the study. Therefore, we will remove this sentence. level of groundwater has been shown by numerous studies in the past to influence the mechanisms behind landslide formation significantly (Miao and Wang, 2023; Preisig, 2020). ~~Consequently, in this study, groundwater levels will serve as inputs for models designed to predict landslides.~~ In pursuing a generalized approach to landslide forecasting, researchers have determined that the critical factors associated with slope instability exhibit temporal variability, necessitating using time series
54: editorial suggestion – can remove “In	The phrase “In contemporary times” has been

contemporary times”	removed according to the reviewer's suggestion. One of the most effective solutions for constructing models to predict time series data involves applying data-driven techniques. The advancement of computational capabilities has driven the widespread adoption of data-driven machine-learning models over physics-based models. This shift is based on the premise that the data used for slope monitoring originates from nonlinear systems (Zhou et al., 2018). ~~In contemporary times,~~ An increasing array of novel data-driven solutions is being developed to overcome the constraints of traditional machine-learning approaches. Among these data-driven solutions, convolutional neural networks (CNNs) have emerged as one of the most effective methods. These CNN models, which excel at automated feature extraction, can enhance efficiency in analyzing complex datasets and improve the accuracy of prediction results (Alzubaidi et al., 2021).
55: CNN has not been defined before the introduction of this acronym	We have added an additional sentence beforehand to clearly explain the abbreviation 'CNN' and to further elaborate on the paragraph's content. One of the most effective solutions for constructing models to predict time series data involves applying data-driven techniques. The advancement of computational capabilities has driven the widespread adoption of data-driven machine-learning models over physics-based models. This shift is based on the premise that the data used for slope monitoring originates from nonlinear systems (Zhou et al., 2018). ~~In contemporary times,~~ An increasing array of novel data-driven solutions is being developed to overcome the constraints of traditional machine-learning approaches. Among these data-driven solutions, convolutional neural networks (CNNs) have emerged as one of the most effective methods. These CNN models, which excel at automated feature extraction, can enhance efficiency in analyzing complex datasets and improve the accuracy of prediction results (Alzubaidi et al., 2021).
64: The term “predict deep-seated landslides” sounds vague. Predicting incipient failure? Reactivation of an already-established failure? Please specify.	We fully agree that the term “predict deep-seated landslides” is unclear. We will revise this term to “predict deep-seated displacement”. Leveraging the effective methodologies mentioned above, this study employs AI models optimized by an innovative metaheuristic optimization algorithm to predict deep-seated ~~landslides~~ displacement on the northern slope of Lushan Mountain in ~~Ren’ai~~ Ren'ai Township, Nantou County. The geological
65-66: Please list references of pre-existing work that you are referencing here	Thank you to the reviewer for this comment. It was an oversight on our part not to include the relevant references to support this point. We have now added the appropriate references, as shown below. the northern slope of Lushan Mountain in ~~Ren’ai~~ Ren'ai Township, Nantou County. The geological characteristics of this area have undergone extensive research (Wang et al., 2015; Lin et al., 2020). Previous studies have identified varying depths of the shear plane. Specifically, Wang et al. determined the depth of the shear plane is 85m and 106m based on inclinometer data (Lin et al., 2020).This research paper is firmly grounded in empirical evidence meticulously collected over eight years from
67: Impressive! At what depth is the failure plane for each of these extensometers?	The geology and shear planes of the Lushan Mountain region have been studied previously, revealing shear planes at depths of 85m and 108m. We have incorporated this information into the manuscript as suggested by the reviewer. the northern slope of Lushan Mountain in ~~Ren’ai~~ Ren'ai Township, Nantou County. The geological characteristics of this area have undergone extensive research (Wang et al., 2015; Lin et al., 2020). Previous studies have identified varying depths of the shear plane. Specifically, Wang et al. determined the depth of the shear plane is 85m and 106m based on inclinometer data (Lin et al., 2020).This research paper is firmly grounded in empirical evidence meticulously collected over eight years from research area and shows the distribution of four survey boreholes (G20, G21, G18, and G25) along the slope. Regolith, slate, and meta-sandstone are three distinct lithological units revealed through drilling. Additionally, the study by Lin et al. identified the depths of failure planes in these survey boreholes. Specifically, boreholes G18 and G25 did not record any failure planes, while boreholes G20 and G21 recorded failure planes at depths of 85 meters and 106 meters, respectively. These failure planes were identified based on inclinometer data from the corresponding study (Lin et al., 2020). Initially, the thickness of the topmost regolith layer was found to be less than 10 meters. Secondly, slate predominated, exhibiting a notable presence with sporadic evidence of weathering that resulted in
88-92: This section feels quite under-referenced, as there are numerous theoretical and observational examples of groundwater impacts on deep-seated	We fully agree with the reviewer's comment. Accordingly, we have included examples from both theoretical and observational studies to clarify this

landslide failure.	point. 101 Casimiro, 2023; Jones et al., 2023). Among these, hydrological conditions, especially groundwater levels, 102 have been one of the most critical elements considered in studies related to landslide prediction. Numerous 103 studies have substantiated this point. For instance, research by Take et al. demonstrated that the distance 104 and velocity of landslides triggered under high antecedent groundwater conditions are significantly more 105 significant compared to scenarios with drier conditions (Take et al., 2015). Another study has shown that 106 the accumulation of water at a soil-bedrock contact can develop of positive pore water pressures, causing 107 landslides (Matsushi and Matsukura, 2007) (see Figure 1). Moreover, studies on past landslide events have 108 also demonstrated similar findings. ~~example~~ Examples of this research include the Tessina landslide in 109 northeastern Italy, where groundwater conditions triggered movement (Petley et al., 2005). Additionally, 110 the study by Keqiang et al. on water-induced landslides in the Three Gorges Reservoir project area 111 highlights the significant impact of hydrological conditions on the likelihood of such disasters (Keqiang 112 et al., 2015).
93-94: This is another purely editorial comment, but the citation style presented here could be more succinct. For example, "Similarly, Preisig (2020) developed…" rather than "Similarly, Presig developed a groundwater prediction… (Presig, 2020)." This same style is utilized throughout the manuscript	We fully agree with the reviewer's suggestion and have revised the citation at this location to make it more concise. 113 Similarly, Preisig (2020) developed a groundwater prediction model for analyzing the stability of a 114 compound slide in the Jura Mountains ~~(Preisig, 2020)~~. Additionally, Srivastava et al. explored machine In addition, we have used the citation style suggested by the reviewer for similar cases throughout the manuscript. 76 Previous studies have identified varying depths of the shear plane. Specifically, Lin et al. (2020) 77 determined the depth of the shear plane is 85m and 106m based on inclinometer data .This research paper 102 have been one of the most critical elements considered in studies related to landslide prediction. Numerous 103 studies have substantiated this point. For instance, research by Take et al. (2015) demonstrated that the 104 distance and velocity of landslides triggered under high antecedent groundwater conditions are 105 significantly more significant compared to scenarios with drier conditions. Another study has shown that 109 northeastern Italy, where groundwater conditions triggered movement (Petley et al., 2005). Additionally, 110 the study by Keqiang et al. (2015) on water-induced landslides in the Three Gorges Reservoir project area 111 highlights the significant impact of hydrological conditions on the likelihood of such disasters ~~(Keqiang~~ 112 ~~et al., 2015)~~. 113 Similarly, Preisig (2020) developed a groundwater prediction model for analyzing the stability of a 114 compound slide in the Jura Mountains ~~(Preisig, 2020)~~. Additionally, Srivastava et al. (2020) explored 115 machine learning algorithms to forecast rainfall and established thresholds for landslide probabilities 116 ~~(Srivastava et al., 2020)~~. Although the research by Srivastava et al. did not directly rely on groundwater 122 heavy rainfall events. Lin et al. (2020) conducted in-depth studies on the mechanisms of landslide 123 occurrence based on the geological conditions of the area ~~(Lin et al., 2020)~~. While successfully providing 141 For instance, Crosta and Agliardi (2003) analyzed the geology and rock mass behavior using 142 Voight's semi-empirical failure criterion, incorporating time-dependent factors to generate velocity curves 143 that indicate risk levels ~~(Crosta and Agliardi, 2003)~~. Recently, Xu et al. (2018) utilized real-time remote 144 monitoring systems to measure internal stress, deep displacement, and surface strain. This data was used 145 to formulate forecasting models to assess slope stability, particularly in railway construction ~~(Xu et al.,~~ 146 ~~2018)~~. However, a common challenge with this method is the instability and frequent changes in the terrain 155 reservoir in Italy (Mufundirwa et al., 2010). In another study, Wu (2010) employed the numerical 156 discontinuous deformation analysis method to simulate a blocky assembly's post-failure behavior, 157 incorporating earthquake seismic data ~~(Wu, 2010)~~. ~~Meanwhile~~ Another study follow this trend by Jiang 158 et al. (2011), who utilized fluid-solid coupling theory to simulate displacement and capture ~~capturing~~ the 159 interaction between fluid and solid materials ~~(Jiang et al., 2011)~~. However, both numerical models and 165 acting on ~~a~~ slope behavior. Fu and Liao (2010) presented a technique for implementing the non-linear 166 Hoek-Brown shear strength reduction, determining the correlation between normal and shear stress based 167 on the Hoek-Brown criterion ~~(Fu and Liao, 2010)~~. Subsequently, the micro-units (microscopic 184 maps depicting landslide susceptibility. For instance, Margarint et al. (2013) employed a logistic 185 regression model to predict landslides based on discrete data in four regions of Romania ~~(Margarint et~~ 186 ~~al., 2013)~~. The logistic regression model yielded promising predictions, with an AUC value (area under 188 utilized to construct a map of landslide susceptibility in the study area. In a similar study, Pham et al. 189 (2016) utilized multiple AI models, including support vector machines (SVM), logistic regression (LR), 190 ~~Fisher 's~~ Fisher's linear discriminant analysis (FLDA), Bayesian network (BN), and naïve Bayes (NB), for 191 landslide susceptibility assessment in a region within the Uttarakhand state of India ~~(Pham et al., 2016)~~. 230 temporal data. For instance, Dahal et al. (2024) utilized spatial-temporal data to pinpoint where landslides 231 may occur and predict when they might happen and the expected landslide area density per mapping unit 232 ~~(Dahal et al., 2024)~~. The Ensemble Neural Network employed in this research yielded promising 238 optimization algorithms optimize the hyperparameters of AI models. For example, Balogun et al. (2021) 239 studied landslide susceptibility mapping in Western Serbia ~~(Balogun et al., 2021)~~. This research collected 244 Hakim et al. (2022) conducted a study utilizing CNN models optimized by the GWO and imperialist 245 competitive algorithm (ICA) for landslide susceptibility mapping from geo-environmental and topo- 246 hydrological factors in Incheon, Korea ~~(Hakim et al., 2022)~~. This research demonstrates that GWO and

<table>
<tr>
<td></td>
<td>Jaafari et al. (2022) employed an AI model known as the group method of data handling (GMDH) for classification purposes, optimizing it using the cuckoo search algorithm (CSA) and the whale optimization algorithm (WOA). In northwest Iran, they aimed to predict landslides based on various factors, including topographical, geomorphological, and other environmental factors ~~(Jaafari et al., 2022)~~.
In an early study of deep landslides in this area, ~~Lin et al. (~~Lin et al. (2020) reported that the Lushan slope exhibits large-scale deep-seated gravitational slope deformation, characterized by a steep scarp, a
also exhibit inter-cleavage gouges. Further details on this geological information can be found in the study by Lin et al. (2020). These instances highlight the potential for significant geological changes and landslide risk in this region.
level gauges (A-17, A-18-2, A-20, and A-24). The transmission, storage, and processing of data are described in detail in the research of ~~Lau et al. in 2023 (~~Lau et al.~~,~~ (2023).
Similar to the machine learning models, in this section, the time series deep learning models will also be trained with default hyperparameters, as found in research of ~~Chou and Nguyen's research in 2023~~ Chou and Nguyen (2023). The performance results of these models are shown in Table 7. Overall, akin to</td>
</tr>
<tr>
<td>103-105: In what way did Lin et al. “somewhat overlook” the importance of hydrological conditions in landslide formation here? Please be specific.</td>
<td>In fact, the research by Lin et al. has accounted for hydrological conditions in landslide formation. Therefore, we have revised the motivation section accordingly. Our research will incorporate the use of AI models to predict deep-seated displacement at Lushan Mountain, a task that has not yet been addressed by previous studies about landslides in this area.
heavy rainfall events. Lin et al. (2020) conducted in-depth studies on the mechanisms of landslide occurrence based on the geological conditions of the area ~~(Lin et al., 2020)~~. While successfully providing valuable insights into the evolution of deep-seated gravitational deformations, ~~their research somewhat overlooked the importance of hydrological conditions and groundwater levels in landslide formation,~~ their study focuses exclusively on employing traditional analytical methods in geological research, such as analyzing data from geotechnical instruments and conducting geological borehole analysis.
Our research aims to adopt a novel approach compared to previous landslide studies at Lushan Mountain by utilizing AI models and metaheuristic optimization algorithms. This research will utilize ~~To address the limitations of previous landslide research in the Lushan Mountain area, this study will explore using~~ ~~hydrological~~ weather conditions and groundwater levels as inputs for AI models to predict deep-seated displacement, thus aiding in landslide forecasting in this region.</td>
</tr>
<tr>
<td>110 (Figure 1). Where is the actual landslide here? Below the diagram? I find the arrow below the right diagram very confusing and vague. A schematic failure plane perhaps informed by the borehole data would be useful for clarifying what it is the authors are trying to illustrate here.</td>
<td>We have revised Figure 1 by removing the arrow and the text 'deep-seated slope failure,' and adding a label for the 'failure plane.' We hope these modifications meet the reviewer's expectations.
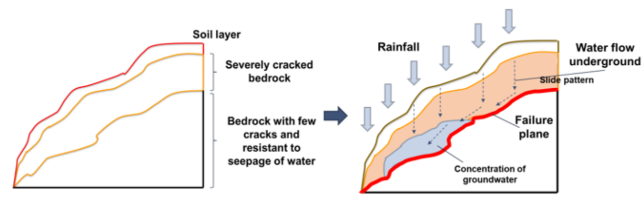

Figure 1. Schematic illustration showing the effects of groundwater on deep-seated slope failure</td>
</tr>
<tr>
<td>122: Numerical models can simulate many scales, not just the laboratory scale. Please fix.</td>
<td>We have revised this section according to the reviewer's suggestion.
Moreover, physical-based numerical and laboratory modeling methods~~, which simulate phenomena at a laboratory scale,~~ are also gaining traction in landslide research. These methods aim to maintain forecasts using various data types while reducing human workload and ensuring high accuracy. For example, Mufundirwa et al. conducted a laboratory study to examine the effectiveness of the inverse</td>
</tr>
<tr>
<td>125: Does this Mufundirwa et al. reference also utilize a numerical model? If not, this paragraph should perhaps speak to both laboratory and numerical studies.</td>
<td>We have revised this paragraph to include references to both laboratory and numerical studies, as suggested by the reviewer.
Moreover, physical-based numerical and laboratory modeling methods~~, which simulate phenomena at a laboratory scale,~~ are also gaining traction in landslide research. These methods aim to maintain forecasts using various data types while reducing human workload and ensuring high accuracy. For example, Mufundirwa et al. conducted a laboratory study to examine the effectiveness of the inverse</td>
</tr>
</table>

130: editorial – can delete “Meanwhile,” here	We have removed the term 'Meanwhile' and revised the sentence accordingly, as suggested by the reviewer. reservoir in Italy (Mufundirwa et al., 2010). In another study, Wu (2010) employed the numerical discontinuous deformation analysis method to simulate a blocky assembly's post-failure behavior, incorporating earthquake seismic data ~~(Wu, 2010)~~. ~~Meanwhile~~ Another study follow this trend by Jiang et al. (2011), who utilized fluid-solid coupling theory to simulate displacement and capture ~~capturing~~ the interaction between fluid and solid materials ~~(Jiang et al., 2011)~~. However, both numerical models and laboratory modeling methods require substantial effort from researchers. These approaches demand deep
135-136: What are “micro-units” here?	“micro-units” refer to microscopic components of the rock mass, a term delineated during the referenced study. We have added a concise explanation to clarify the meaning of this term in the manuscript: acting on a slope behavior. Fu and Liao (2010) presented a technique for implementing the non-linear Hoek-Brown shear strength reduction, determining the correlation between normal and shear stress based on the Hoek-Brown criterion ~~(Fu and Liao, 2010)~~. Subsequently, the micro-units (microscopic components of the rock mass) instantaneous friction angle and cohesive strength under specific stress conditions are calculated. Although this approach effectively addresses cost and labor issues, it still
140-142: The previous paragraphs have not demonstrated that these “conventional methods have shown limited success in handling big data…” More information needs to be provided in this or the previous paragraphs to provide justification for this argument.	The assertion that conventional methods show limited success in handling big data is not entirely complete or accurate. We have added more information in this section to explain the drawbacks of conventional methods and the necessity of using AI models in this research. that indicate risk levels ~~(Crosta and Agliardi, 2003)~~. Recently, Xu et al. (2018) utilized real-time remote monitoring systems to measure internal stress, deep displacement, and surface strain. This data was used to formulate forecasting models to assess slope stability, particularly in railway construction ~~(Xu et al., 2018)~~. However, a common challenge with this method is the instability and frequent changes in the terrain and geology of landslide-prone areas. This necessitates constant updates to the computational model, which can be time-consuming and labor-intensive. Moreover, physical-based numerical and laboratory modeling methods~~, which simulate phenomena at a laboratory scale,~~ are also gaining traction in landslide research. These methods aim to maintain reservoir in Italy (Mufundirwa et al., 2010). In another study, Wu (2010) employed the numerical discontinuous deformation analysis method to simulate a blocky assembly's post-failure behavior, incorporating earthquake seismic data ~~(Wu, 2010)~~. ~~Meanwhile~~ Another study follow this trend by Jiang et al. (2011), who utilized fluid-solid coupling theory to simulate displacement and capture ~~capturing~~ the interaction between fluid and solid materials ~~(Jiang et al., 2011)~~. However, both numerical models and laboratory modeling methods require substantial effort from researchers. These approaches demand deep expertise and the development of complex models. More importantly, they rely heavily on assumptions during the simulation process and may not accurately reflect real-world conditions, leading to significant errors. Stability analysis is another commonly used method related to physics, which evaluates the forces acting on a slope behavior. Fu and Liao (2010) presented a technique for implementing the non-linear Hoek-Brown shear strength reduction, determining the correlation between normal and shear stress based on the Hoek-Brown criterion ~~(Fu and Liao, 2010)~~. Subsequently, the micro-units (microscopic components of the rock mass) instantaneous friction angle and cohesive strength under specific stress conditions are calculated. Although this approach effectively addresses cost and labor issues, it still heavily relies on the ~~researcher's~~ researcher's assumptions and is limited by the ability to utilize only a small portion of data from the research area. However, in landslide studies, monitoring data is constantly updated, generating large volumes daily with a temporal relationship (Peternel et al., 2022; Corominas et al., 2014). ~~Hence, conventional methods have shown limited success in handling big data, especially in identifying highly intricate samples that require analysis of time series relationships or complex nonlinear associations.~~ As previously mentioned, using conventional methods in landslide research presents numerous challenges whenever data changes or gets updated. In contrast, AI models can overcome these difficulties by automatically learning to identify connections between input and output data. AI models can be updated to incorporate additional input variables and handle increasing amounts of data flexibly in response to real-world conditions. Therefore, AI models will be utilized in this research instead of conventional methods.
154: Is there any discussion on why this model was	Pham et al. (2016) did not explain why the support

the most successful?	vector machine (SVM) model provided the most accurate predictions compared to other models. They simply noted that the superior performance of the SVM model was consistent with conclusions from numerous past studies. From our perspective, the study by Pham et al. did not employ methods to search for optimal hyperparameters to minimize the errors of the AI models (such as grid search or metaheuristic optimization algorithms). This oversight resulted in the models not operating under optimal conditions. Consequently, determining the truly effective model in their study remains challenging. Therefore, in the reference section of our current research, we can only mention the SVM as the most effective model according to their conclusions without further explanation due to the lack of optimization methods. We hope the reviewers understand this challenge we face.
163-164: Please define what the term “feature engineering” is here	Adding further explanation for the term "feature engineering" will enhance readers' understanding of this study. We have included the requested annotation below as per the reviewer's suggestion. interrelationships, mainly when data availability is limited (Zhang et al., 2020). Finally, feature engineering (the process of selecting and transforming input variables to enhance the performance of the models) is computationally intensive and labor-intensive, limiting its applicability when rapid forecasting is required.
166: these parameters (topographic slope and soil parameters) don’t necessarily have to be one-dimensional. Topography can be 2-D and soil parameters can be 3-D (and perhaps even time-dependent). 168-169: from my limited understanding of AI-based models, most are black boxes and therefore disentangling physical processes can be difficult. I thought this was the domain of physics-informed neural networks?	We fully agree with the reviewer's comments regarding the inaccuracies in this paragraph. We have revised the paragraph as follows: ~~Given that slope profiles and soil parameters are one-dimensional variables,~~ Alongside the aforementioned machine learning models, a range of neural network models, from simpler ones like Artificial Neural Networks (ANN) to more advanced approaches such as Deep Neural Networks (DNNs) and CNN ~~can~~ are also ~~be~~ employed in research related to landslide (Kumar et al., 2017; Zheng et al., 2022) ~~to uncover the relationship between slope stability and input parameters with minimal computational overhead (Fu et al., 2022).~~ Notably, CNN models have become increasingly popular and are widely used in research related to this disaster. CNN models often yield superior predictive results than other models in landslide susceptibility assessment and displacement prediction (He et al., 2024). ~~Additionally, CNN models have been used in studies of this disaster. While CNN was initially designed for image processing, its input and internal architecture are tailored for two-dimensional matrices, including the convolution kernel and feature map. To address the one-dimensional nature of slope profiles and soil physical and mechanical parameters, Pei, Meng, & Zhu developed a 1D-CNN model with dynamic inputs to account for time-varying trigger factors (Pei et al., 2021). Their approach demonstrated superior performance to conventional machine learning models regarding accuracy and robustness. However, it's worth noting that this approach has yet to gain widespread adoption.~~
184: “predicting landslide displacement” would be more specific here	We have revised the term “landslide prediction” to “predicting landslide displacement” according to the reviewer's request. employs a combination of machine learning methods, time-series deep learning, and CNN models to compare and determine the most suitable model for predicting landslide displacement ~~prediction~~. Therefore, our research aims to address this gap.
Section 3.1 (Lines 218-277): This part confused me at first because CNN’s deal with imagery and you	We fully agree with the reviewer's comment and have added a paragraph to further elaborate on this

<table>
<tr>
<td>are using time series vectors. It is later clarified in the paper that the time series data are converted to images for use with the models, but it would be worth stating something up front that vector data can also be utilized in this construct with the prop</td>
<td>point, as detailed below.

CNN models are typically used for image processing tasks. However, the input data for this study is in numerical and vector form. Therefore, several transformation steps are required to convert this numerical and vector data into image data suitable for CNN input. Detailed information about these transformation steps can be found in the study by Chou and Nguyen 2023 (Chou and Nguyen, 2023).</td>
</tr>
<tr>
<td>250 (Fig. 3): the 3x3 kernel illustrated here is mislabeled as 2x2</td>
<td>The incorrect annotation of the kernel has been corrected in the revised version of this figure.

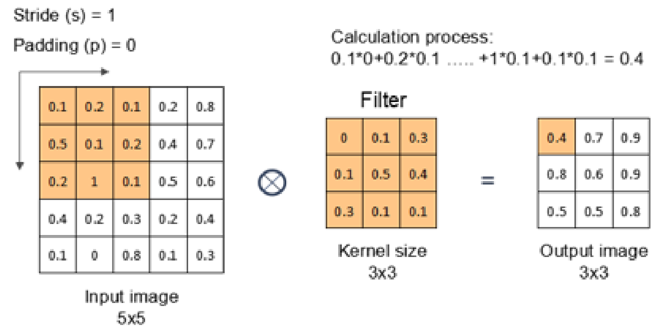

Figure A-2. Processing flow in convolution layer.</td>
</tr>
<tr>
<td>292: It’s not clear here why RNNS are well-suited to learning time series with short-term dependencies. Please clarify.</td>
<td>We have provided additional reasoning as to why RNNs are well-suited for learning time series with short-term dependencies, as requested by the reviewer.

hidden layer; b is the bias term; and tanh() represents the hyperbolic tangent activation function, i.e., $tanh(x) = \frac{1-e^{2x}}{1+e^{2x}}$. The mechanism of learning over time steps, stored within cells, enables RNNs to capture complex relationships between cells and time sequences effectively. However, as the duration of dependencies increases, RNN models are susceptible to issues related to vanishing gradients (Bengio et al., 1994). Therefore, RNNs are well-suited to learning time series involving short-term dependencies.</td>
</tr>
<tr>
<td>318-322 (Performance Metrics): If you are assigning a separate section to performance metrics, it would be good to describe what each one is and the benefits and drawbacks for each metric.</td>
<td>We greatly appreciate this feedback from the reviewer. Performance metrics serve as evaluation criteria for AI models in this study. Providing comprehensive information about them will enhance readers' understanding of this research. Therefore, we have incorporated detailed information about these performance metrics in Section 3.4.2 as follows:

3.4.2 Performance Metrics
This study utilized four widely recognized performance measures to assess the ~~model’s~~ model's effectiveness in prediction accuracy (Chou and Nguyen, 2023). The measures included mean absolute error (MAE), mean absolute percentage error (MAPE), and root mean square error (RMSE).
MAE represents the mean of absolute errors, calculated as the average of the absolute differences between actual and predicted values. Its advantage lies in its simplicity, which provides a straightforward measure of average prediction error. However, a drawback of MAE is its insensitivity to more significant errors, so it may not effectively highlight differences between models when significant errors are present. It is defined as:
$MAE = \frac{1}{n}\sum_{i=1}^{n}|y_i - \hat{y}_i|$ (5)
where n is the number of predictions, y_i is the i^{th} forecasted value, and $\hat{y}_i$ is the corresponding i^{th} actual value.
MAPE quantifies the average absolute error ratio—derived from the differences between actual and forecasted values—to the actual value. It provides a clear metric in percentage terms, facilitating straightforward interpretation across various datasets. However, MAPE's limitation arises from its sensitivity to zero values in the actual data, which can become undefined or impractical to compute, limiting its utility in scenarios involving zero or near-zero actual values. The expression for MAPE is as follows:</td>
</tr>
</table>

	$$MAPE = \frac{1}{n}\sum_{i=1}^{n}\left|\frac{y_i-\hat{y}_i}{y_i}\right| \quad (6)$$ where n is the number of predictions, y_i is the i^{th} forecasted value, and $\hat{y}_i$ is the corresponding i^{th} actual value. RMSE represents the square root of the average squared error between actual and forecasted values and is widely used for its ability to indicate the dispersion of errors. This method captures the magnitude and direction of errors, making it practical for assessing overall prediction accuracy. However, RMSE tends to be more sensitive to outliers and significant errors than MAE due to its squaring of errors during computation. This sensitivity can disproportionately affect its evaluation in datasets with extreme values. The expression for RMSE is as follows: $$RMSE = \sqrt{\frac{1}{n}\sum_{i=1}^{n}(y_i-\hat{y}_i)^2} \quad (7)$$ where n is the number of predictions, y_i is the i^{th} forecasted value, and $\hat{y}_i$ is the corresponding i^{th} actual value.
328: What exactly is a particle in this instance? Some context is needed here.	We fully agree with the reviewer's comment. Our manuscript lacked sufficient detail regarding the term 'particle.' We have now added an explanatory section on this term in Section 3.5. **3.5 Age of Exploration-Inspired Optimizer** This study employs a range of AI models to forecast deep-seated displacement in mountainous regions. To enhance the prediction accuracy of these AI models, the study incorporates a novel metaheuristic optimization algorithm known as the Age of Exploration-Inspired Optimizer (AEIO). Developed by Chou and Nguyen in 2024, this algorithm has demonstrated high effectiveness in fine-tuning the hyperparameters of AI models. This algorithm treats each particle in the search domain as an explorer. The movement of particles toward regions with higher fitness values parallels the exploratory activities of the Age of Exploration, where explorers sought ideal locations for establishing colonies. In this study, each particle represents a set of hyperparameters, with the ultimate goal of the search process being to identify the optimal particle or hyperparameter set that minimizes prediction error for AI models. Figure 3 illustrates the AEIO algorithm.
337 (Fig. 8): The red arcuate arrows that link the positional strategies appears to suggest that once one strategy is selected, the explorer goes from one strategy to the next when in fact they return to the middle after each time step (correct?). If that is the case, then the arrows should arc back down to the central location to reflect the decision-making process that occurs with each positional change.	We have revised the illustrative figure for the AEIO algorithm. Specifically, we removed the red arcuate arrows linking the positional strategies to prevent any misunderstanding for the reader. Additionally, we added bidirectional arrows from the action of choosing the strategy to each colony search action. Furthermore, we included arrows around the central image of the explorer-choosing a strategy, indicating that the search process repeats with each iteration. 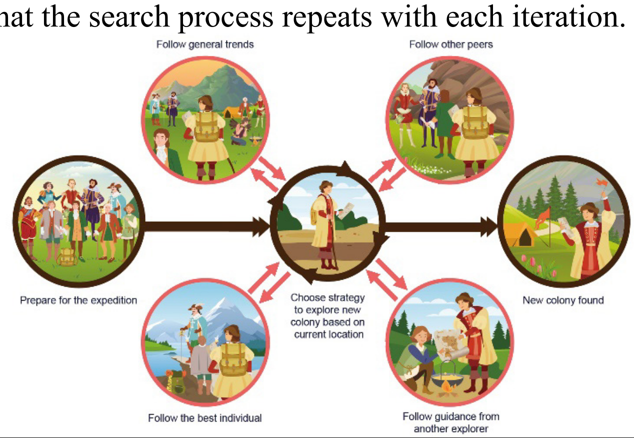
361-372: These two steps need to be elaborated on a little bit more, as it is presented somewhat confusingly and the equations for (8) and (9) are identical.	We acknowledge that the two equations mentioned above are quite similar. The only difference between them lies in the values $x_{i,d}(t)$ and $x_{1,d}(t)$. Despite this slight variation in the formula, the mechanisms of the two movements are fundamentally different.

	One equation guides the current particle towards the best particle, while the other directs the current particle in a direction based on the distance of a random particle from the best one. We have added annotations in the explanations of the formulas. These annotations clearly specify the mathematical notation for each type of particle in the explanations. We hope that this addition will make the movement mechanisms of the particles more comprehensible. • **Explorers follow general trends** The explorer choosing this movement type will calculate the distance from their location $x_{i,d}(t)$ to the center of all other explorers $(Meanvl_d(t))$, then attempt to move towards that central point in the hope of finding a better location with the potential to establish a new colony. The following formula determines the explorer's position after the movement: $x_{i,d}(t+1) = x_{i,d}(t) + \alpha * \left(Meanvl_d(t) - x_{i,d}(t)\right) \times rand(0,1) \times R$ (8) $Meanvl_d(t) = \frac{x_{1,d}(t)+x_{2,d}(t)+\dots+x_{n_{Pop},d}(t)}{n_{Pop}}$ (9) where $d = 1,2, \dots D$; D is the number of dimensions; $i = 1,2, \dots n_{Pop}$; n_{Pop} is the total number of explorers; $t = 1,2, \dots MaxIt$ is the number of iterations; $MaxIt$ is the maximum value of iteration; α is a parameter for adjusting the particle's movement toward the centroid position (usually equals 3). $Meanvl_d(t)$ is the centroid of all particles in dimension d. $rand(0,1)$ is the random number in the range [0,1]. R: a number that equals 1 or 2 depending on the value of rand(0, 1) per the equation. $R = round(1 + rand(0,1) \times 1)$, $x_{i,d}(t)$ is the location of particle i in iteration t, $x_{i,d}(t+1)$ is the location of particle i in iteration $(t+1)$. • **Explorers follow three other peers** Explorers employing this movement method will calculate the average position of three randomly selected other explorers $\left(\frac{x_{1,d}(t)+x_{2,d}(t)+x_{3,d}(t)}{3}\right)$ and then move toward this newly calculated average position. The explorer's new position is computed using the following formula: $x_{i,d}(t+1) = x_{i,d}(t) + \left(\frac{x_{1,d}(t)+x_{2,d}(t)+x_{3,d}(t)}{3} - x_{i,d}(t)\right) \times rand(0,1) \times R$ (10) where: $x_{1,d}(t)$, $x_{2,d}(t)$ and $x_{3,d}(t)$ are three random explorers in dimension d at iteration t, $d = 1,2, \dots D$; D is the number of dimensions; $i = 1,2, \dots n_{Pop}$; n_{Pop} is the total number of explorers; $t = 1,2, \dots MaxIt$ is the number of iterations; $MaxIt$ is the maximum value of iteration. • **Explorers follow the best one** According to this strategy, the explorer $(x_{i,d}(t))$ will move closer to the position of another explorer currently holding the best position $(Best_d(t))$, as determined by the following formula: $x_{i,d}(t+1) = x_{i,d}(t) + \left(Best_d(t) - x_{i,d}(t)\right) \times rand(0,1) \times R$ (11) where: $Best_d(t)$ represents the position of the particle with the best fitness in dimension d at iteration t, the parameters d and t hold the same significance as defined in Equation 10. • **Explorers follow guidance from another one** Explorers in favorable positions with access to information can execute this movement strategy. In this scenario, explorers $(x_{i,d}(t))$ will consult with ~~each other~~ another explorer. The consulted explorer will compare their direction and distance to the best individual, who holds the most favorable position $(Best_d(t))$ and guide the inquirer. This algorithm assumes that the inquirer can be any explorer, i.e., a random explorer $(x_{1,d}(t))$. The following formula describes how to calculate the new position of the explorer following this strategy: $x_{i,d}(t+1) = x_{i,d}(t) + \left(Best_d(t) - x_{1,d}(t)\right) \times rand(0,1) \times R$ (12) where: $x_{1,d}(t)$ is a random explorer in dimension d at iteration t. the parameters d and t hold the same significance as defined in Equation 10.
388 (Fig. 10): Much more information is needed in the figure caption here, as the current captions are essentially vacant. Additionally, the map in (a) is missing crucial information such as latitude and longitude graticules, and contains extraneous information (e.g., random text and other symbols that are not defined). With regard to (b), was the landslide failure plane identified with these cores? Or is the failure plane depth only known in the	We have made several adjustments to Figure 10 and Figure 11. Specifically, in Figure 10, we have added information on latitude and longitude. Additionally, we have removed unnecessary details (e.g., random text and undefined symbols) from Figure 10.

<table>
<tr>
<td>extensometer boreholes? Please provide more information here or elsewhere in the manuscript.</td>
<td>
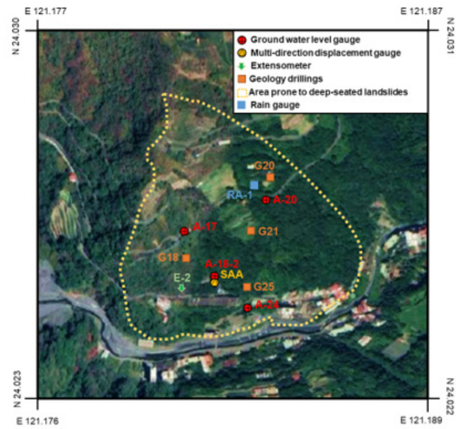

Image source: Imagery ©2022 CNES/Airbus, Maxar Technologies, Map data ©2022 Google

Figure 5. Locations of measurement devices

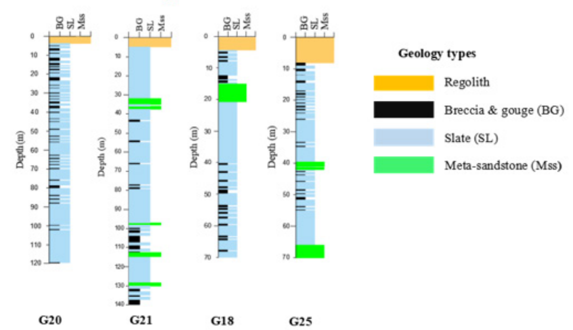

Figure 6. Illustration of geological drilling survey

For Figure 11, we primarily use this image to provide readers with geological information about the area.

These survey boreholes utilize data inherited from the study by Lin et al. (2020), which provides a detailed account of the failure plane depths. We have included information on the depth of the failure planes for each survey borehole in the manuscript and added a citation to the previous study, allowing readers to seek further details on these surface plane determinations.

research area and shows the distribution of four survey boreholes (G20, G21, G18, and G25) along the slope. Regolith, slate, and meta-sandstone are three distinct lithological units revealed through drilling. Additionally, the study by Lin et al. identified the depths of failure planes in these survey boreholes. Specifically, boreholes G18 and G25 did not record any failure planes, while boreholes G20 and G21 recorded failure planes at depths of 85 meters and 106 meters, respectively. These failure planes were identified based on inclinometer data from the corresponding study (Lin et al., 2020).

Initially, the thickness of the topmost regolith layer was found to be less than 10 meters. Secondly,
</td>
</tr>
<tr>
<td>407: Please cite the previous research here</td>
<td>
We have added additional citations in this paragraph as per the reviewer's request.

Previous research has detected signs of brittle deformation in the area. These indications include chevron folds within cleavages, visible cracks, and intricate jigsaw puzzle-like patterns at the head of the rock formations. Overturned and flexural toppling cleavages are prevalent toward~~s~~ the toe of the slope. Additionally, kink bands are observable on ~~cleavages~~ fractures ~~that have recently undergone~~ recently undergoing flexural folding along the eastern boundary. Notably, horizontal cleavages near the toe region also exhibit inter-cleavage gouges. Further details on this geological information can be found in the study by Lin et al. (2020). These instances highlight the potential for significant geological changes and landslide risk in this region.
</td>
</tr>
</table>

<table>
<tr>
<td>407-412: I think the term “cleavage” is misused here. Do the authors mean “fracture”? Typically, cleavage refers to the tendency of a mineral to break along planes defined by crystal lattice structure and are typically not seen at the scale of an entire hillslope. Lastly, it would be worth putting these observation zones on the map of the landslide for reference.</td>
<td>We greatly appreciate the reviewers for this suggestion; we fully agree that the term “fracture” is more appropriate than “cleavage” and we have made the corresponding change.

Previous research has detected signs of brittle deformation in the area. These indications include chevron folds within cleavages, visible cracks, and intricate jigsaw puzzle-like patterns at the head of the rock formations. Overturned and flexural toppling cleavages are prevalent towards the toe of the slope. Additionally, kink bands are observable on ~~cleavages~~ fractures ~~that have recently undergone~~ recently undergoing flexural folding along the eastern boundary. Notably, horizontal cleavages near the toe region also exhibit inter-cleavage gouges. Further details on this geological information can be found in the study by Lin et al. (2020). These instances highlight the potential for significant geological changes and landslide risk in this region.

In response to the suggestion to display observation zones on the map, we have included them in Figure 10. In addition to showing the locations of the boreholes and data collection sites, Figure 10 delineates the areas prone to deep-seated landslides, which represent the observation zones.

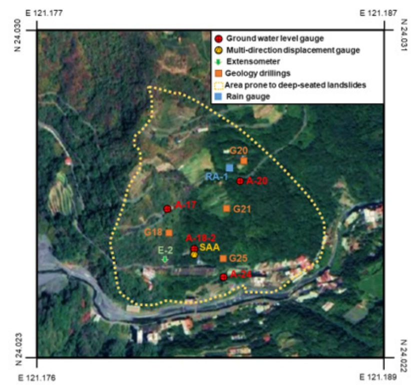

Image source: Imagery ©2022 CNES/Airbus, Maxar Technologies, Map data ©2022 Google
Figure 5. Locations of measurement devices</td>
</tr>
<tr>
<td>426: How was the rainfall data measured? Via a local rain gauge? If so, can put it on the map as well.</td>
<td>Rainfall data for this study were collected using a rain gauge installed on-site. The location of the rain gauge has been annotated on the map in Figure 10.

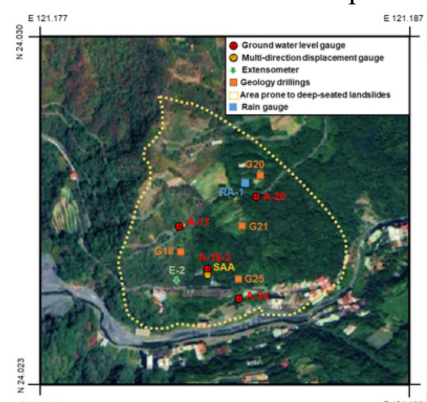

Image source: Imagery ©2022 CNES/Airbus, Maxar Technologies, Map data ©2022 Google
Figure 5. Locations of measurement devices</td>
</tr>
<tr>
<td>438-442 (Figs. 12-14): It is very difficult to compare the time series data as all the axes are scaled differently. I strongly recommend making one three-</td>
<td>We have revised Figures 12-14 as per the author's request. Specifically, we merged all three original figures into one and placed them on a single</td>
</tr>
</table>

panel figure that is aligned in the time dimension instead of three separate figures. I would also recommend putting the known storms from Table 2 as vertical bands on each subplot. This will really help unify the datasets and make it much easier for readers to discern how precipitation, groundwater levels, and landslide displacement are aligned.	timeline. Additionally, we added a graph to depict the precipitation of recorded heavy rainfall in the studied area. Placing all graphs on the same timeline facilitates easier tracking of concurrent data variations for readers. Moreover, it highlights the relationships between different datasets. 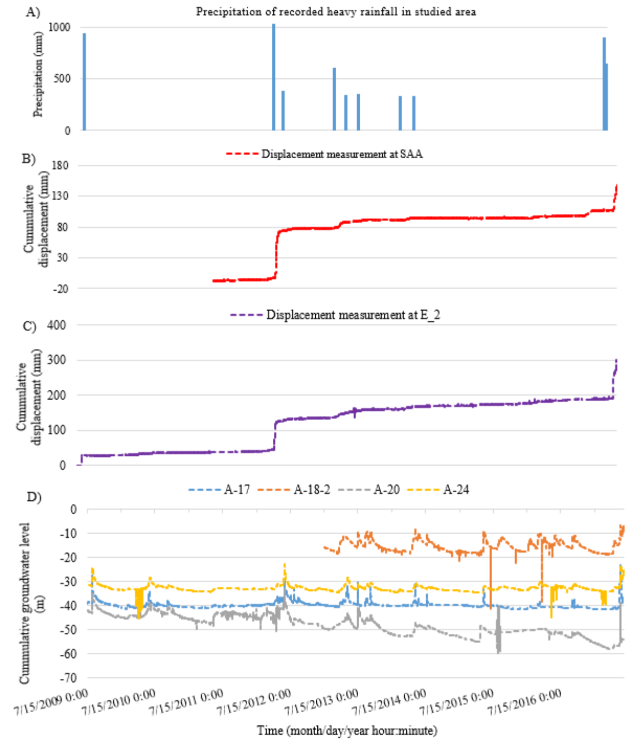 Figure 7. Unified timeline visualization of data in this study. A) Precipitation of recorded heavy rainfall in the studied area; B) Measured displacements from extensometer SAA C) Measured displacements from extensometer E_2; D) Groundwater levels at stations A-17, A-18-2, A-20, and A-24.
446-447: Should be "June" instead of "August", otherwise the groundwater will be responding to a future event!	We sincerely apologize for this confusion. The error is corrected as below. increases coinciding with periods of pronounced fluctuations in groundwater levels. Specifically, in June 2012, there was a notable surge in groundwater levels attributed to heavy rainfall from June 8, 2012, to June 17, 2012, totaling 1029 mm over 219 hours (as indicated in Table 2 and Figure 7A). The abnormal rise in groundwater levels caused a structural alteration in the area's soil, consequently amplifying deep-
457-458: The groundwater levels that are apparently driving displacement here are 10s of meters below the ground surface (e.g., Fig. 14). Which impacts on soil structure by thermal processes are you referring to? Do thermal effects at this depth contribute to landsliding? Please provide context and references here to back up this statement or otherwise remove.	In this study, we incorporated temperature as an input for AI models to predict deep-seated landslides, due to its significant impact on pore water pressure and effective frictional resistance forces, which in turn affects soil strength. We have included several citations from past research to substantiate this argument, as outlined below. In addition to groundwater level data, weather factors such as temperature and humidity are also utilized as input data for the prediction model. This study includes temperature as an input variable for AI models to predict deep-seated displacement due to its impact on soil structure. Elevated temperatures can cause thermal expansion of soil particles, which can increase pore water pressure and reduce effective frictional resistance forces (Pinyol et al., 2018). Additionally, previous research has shown a relationship between temperature and the likelihood of landslides in clay-rich soils, which are also present in the geological composition of Lushan Mountain (Shibasaki et al., 2017; Loche and Scaringi, 2023).~~These factors significantly impact the soil structure and can trigger substantial displacement or landslides~~.

459-461: Please describe more the data used here? For example, is it daily data? What is the grid size? What is the measurement source?	We have provided additional information to help readers better understand the data collected from the website https://power.larc.nasa.gov. This study collected groundwater level and displacement data on-site using sensors. Furthermore, temperature and humidity data were obtained from the website https://power.larc.nasa.gov. This dataset is part of the Prediction of Worldwide Energy Resource (POWER) project, developed by the National Aeronautics and Space Administration (NASA) of the United States. The POWER solar data derives from satellite observations, which are used to infer surface insolation values. Meteorological parameters are sourced from the Modern-Era Retrospective analysis for Research and Applications, Version 2 (MERRA-2) assimilation model. The primary solar data is available with a global resolution of 1° x 1° latitude/longitude, while the meteorological data is provided at a finer resolution of ½° x ⅝° latitude/longitude. Users can download the data hourly, daily, or monthly through this website.
488: Indeed! Having forecast data a week in advance would be extremely beneficial.	We sincerely appreciate the reviewer’s acknowledgment. We hope that these predictive results will contribute to the advancement of forecasting methods, ultimately aiding in the evacuation efforts prior to landslide disasters.
499: Specify process to be modeled (i.e., landslide displacement)	We have corrected this sentence for accuracy, as the focus of the study is on predicting deep-seated displacement rather than deep-seated landslides. **4.1 Model Establishment** Predicting deep-seated displacement ~~landslides~~ at Lushan Mountain is undoubtedly highly challenging, given that such landslides depend on numerous factors. Therefore, multiple methods will be
502: editorial comment – shouldn’t end sentence with “…”	We have removed the ellipsis at the end of this section as requested by the reviewer. Predicting deep-seated displacement ~~landslides~~ at Lushan Mountain is undoubtedly highly challenging, given that such landslides depend on numerous factors. Therefore, multiple methods will be employed simultaneously to identify the optimal AI model for prediction. These methods include single machine learning, time series deep learning, CNN, and hybrid models~~…~~.
509 (Fig. 16): Very helpful flow chart	We sincerely appreciate the reviewer's praise. We consistently strive to use visuals and diagrams to convey our research, aiming to make it more accessible and comprehensible for readers.
545: It would be helpful to have a figure showing a subset of the models plotted alongside the displacement data so readers could see how the differences in MAPE are actually reflected in the time series predictions	We fully agree with the reviewer's suggestion. Including a figure that illustrates the temporal variation in the predicted deep-seated displacements by different models will help readers clearly see how the differences in MAPE are actually reflected in the time series predictions. However, given the extensive number of AI models used in this study, displaying the prediction results of all models would increase the complexity of the charts, making it challenging to discern the differences in the models' performance. Therefore, we have chosen to display the displacement predictions of the most representative models, including the best machine learning model (XGBoost), the best time-series deep learning model (R-GRU), the best CNN model (MobileNet), and the best hybrid models (AEIO-MobileNet and AEIO-R-GRU).

	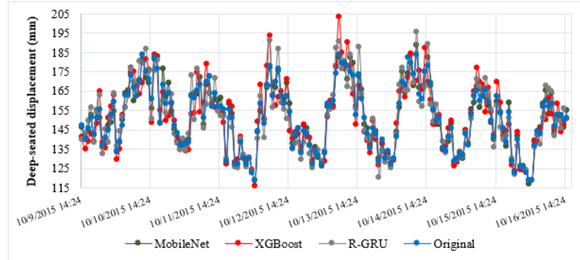 a) Prediction results of deep-seated displacement by single AI models. 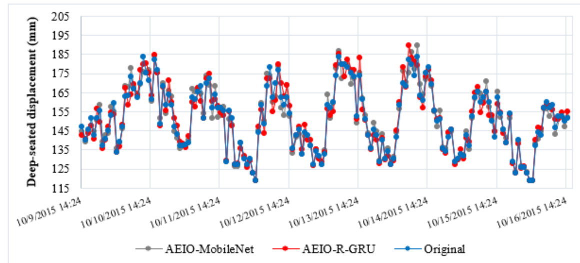 b) Prediction results of deep-seated displacement by AI models optimized using the AEIO algorithm. Figure 10. Graph comparing the real and predicted deep-seated displacement.
568: change "landslides" to "landslide displacement" or something similar	We have revised the term "deep-seated landslide" to "deep-seated displacement" following the reviewer's suggestion. **4.2.2 Best AI Model Finetuned by AEIO Algorithm** This section will focus on fine-tuning the hyperparameters of the numerical model to enhance its performance in predicting deep-seated ~~landslides~~ displacement. The AEIO algorithm will fine-tune the hyperparameters of the study's best numerical AI model, the R-GRU model. Details regarding the names and search ranges of the hyperparameters are outlined in Table 8. The objective function of the AEIO
660-664: This is a nice motivating paragraph that belongs in the introduction and would help provide context for the study.	We agree that including this information in the introduction will help clarify the context of our research and enable readers to better understand the benefits of these predictive models. Therefore, we have incorporated this information into the final paragraph of the introduction. This study represents the first instance of AI models being utilized to predict deep-seated landslides in Lushan Mountain. Additionally, it marks the inaugural application of AEIO for fine-tuning AI models in landslide-related research. Our findings provide a valuable resource for civil engineers, contractors, and inspectors involved in the planning and monitoring ~~of~~ construction projects in landslide-prone areas. Predicting the likelihood of landslide events can help minimize property loss, guide schedule adjustments, improve work safety, and ensure smooth traffic flow during critical periods. Additionally, understanding internal displacements provides engineers with precise data to evaluate the resilience of structures and infrastructure in vulnerable areas, enabling the issuance of prudent warnings.
668-668: Are these models not considered "conventional"? If not, why not? Could also be specified earlier on in the manuscript.	We sincerely apologize for this oversight; the term "conventional" should not be used for CNN models for the following reasons: - "Conventional models" refer to traditional, simple machine learning models such as regression, decision trees, support vector machines, etc. In contrast, CNNs are not traditional methods and have recently become widely used. - CNNs have been shown in numerous studies to yield superior performance compared to other models. Labeling CNNs as conventional models

	may diminish their value and advanced nature, potentially leading to misunderstandings about their applicability. Therefore, we will use the term "standard CNN models" to refer to models other than retrained CNN models. We have added a section to explain this terminology to prevent any confusion for the readers. This study will use various CNN models to predict deep-seated slope displacement. The CNN models employed in this research include VGG (Simonyan and Zisserman, 2014), ResNet (He et al., 2016), Inception (Szegedy et al., 2015), Xception (Chollet, 2016), MobileNet (Howard et al., 2017), DenseNet (Huang et al., 2017), and NASNet (Zoph et al., 2018). To clarify, the term "standard CNN models" will refer to models with structures that can be user-defined, while "retrained CNN models" will denote those with architectures that have been researched and developed by other scientists and have been proven to be highly effective.
678: Here again would be a great place to delve into the "why" a little bit more. Any thoughts why a certain class of models outperforms the others? This discussion section is quite short relative to the rest of this paper, and there are a lot of aspects to potentially discuss. Does withholding certain parameters (e.g., temperature, humidity, or both) impact the results substantially? If so, why might that be the case? Since so much work has been done to get to this stage of predictive success, a small amount of additional work may help elucidate the role of specific processes in aiding the predictability of landslide displacement in this context that could be useful for the broad readership of NHESS.	We have expanded the discussion section to provide a more comprehensive explanation of the study's results. Specifically, we have added reasons to explain why CNN models performed better than both machine learning and time-series deep learning models. Additionally, this discussion highlights a limitation of the study: the lack of analysis on the relative importance of each type of input data for the predictive capabilities of the AI models. This limitation underscores the need for further research to clarify these aspects. of our study lies in adopting pre-trained models, such as MobileNet, DenseNet, Inception, and VGG, rather than ~~conventional~~ standard CNN models. ~~The practicality of employing these pre-trained models has demonstrated effectiveness in predicting displacement in this research.~~ By employing various AI models, this study identifies the most effective model for predicting deep-seated landslides and offers a comprehensive overview of the performance of different AI models. Initially, machine learning models exhibited relatively high prediction errors, with MAPE ranging from 8.14% to 15.19%. This performance was generally lower than time-series deep learning models, which showed MAPEs ranging from 7.9% to 14.73%. The superior performance of the time series deep learning models is attributed to their ability to process sequential data and retain information from previous steps. This enables them to learn patterns from the dataset more effectively than traditional machine learning models. However, compared to CNN models, the results of the time series deep learning models are not as strong. This disparity is attributed to the superior learning mechanism of CNNs. The convolutional and pooling layers in CNNs enable robust feature extraction from the input data. Convolutional layers are particularly effective at identifying complex patterns and subtle features within time series data, primarily when spatial correlations exist. This capability allows CNNs to uncover essential features that other models might overlook. The input data used for the AI models were selected because they significantly influence the likelihood of deep-seated landslides, as detailed in Section 3.6. However, a limitation of this study is that it does not evaluate the relative importance of each input data type on prediction accuracy. Future research should explore the impact of different combinations of input data on AI model performance. This could help identify the significance of each input type and potentially reveal the optimal combination of inputs to enhance prediction accuracy further.

Summary of the Changes to Reviewer 2's Recommendations and Comments

Journal: Natural Hazards and Earth System Sciences

Ref: NHESS-2024-86

Title: Predicting Deep-Seated Landslide Displacements in Lushan Mountains through the Integration of Convolutional Neural Networks and an Age of Exploration-Inspired Optimizer

The authors appreciate the reviewer's valuable feedback. The summary of the changes based on the reviewer's recommendations & comments is listed below. All the revisions are TRACKED in the re-submitted WORD file along with marked RED COLOR for the ease of the reviewer's perusal. Our colleague, a native English speaker of BLUE COLOR, has corrected grammatical and writing style errors in the original version.

Recommendations and Comments of Reviewer	**Authors' Summary of the Changes**
The manuscript can be an interesting contribution for the methodology of use and interpretation of data for the prediction of deep landslide movements. However, it requires a substantial review in the text, in the figures and in the production of additional figures to show the final results. The list presented below are the specific comments:	We are pleased to receive positive feedback from the reviewer on this study. We also sincerely appreciate the reviewer's detailed comments, which have identified the limitations of our research. We have endeavored to revise the manuscript in response to each of the reviewer's comments. The details of these revisions are outlined below.
1) Sections 3.1 and 3.2 should be in the text in more synthetic form, placing much of the content in an appendix	We completely agree with the reviewer's suggestion. Excessive focus on the operational mechanisms of the AI models could distract readers from the primary objective of the study. Therefore, we have moved this content to the appendix. **3.1 Convolutional Neural Networks** In 1998, LeCun introduced a novel type of DNN known as the CNN, specifically designed for processing data with a grid-like structure, such as images. The complex, layered system of CNN facilitates the automated extraction of features without extensive preprocessing, making it ideal for object recognition, image classification, and segmentation tasks. The detailed mechanism of the CNN model can be found in appendix A. ~~The architecture of a typical CNN, as illustrated in Figure 2, comprises an input layer (to receive image data), followed by hidden layers (including convolutional, pooling, and fully connected layers), and concludes with the output layers. As depicted in Figure 2, the complexity of CNN~~ **3.2 Deep Learning Models for Time Series** RNN was introduced by Elman in 1990 (Elman, 1990). This model makes predictions based on sequential data, crucial for language modeling, document classification, and time series analysis. The architecture of an RNN model can be found in appendix B. **APPENDIX** **Appendix A. Convolutional Neural Networks** The architecture of a typical CNN, as illustrated in Figure A-1, comprises an input layer (to receive image data), followed by hidden layers (including convolutional, pooling, and fully connected layers), and concludes with the output layers. As depicted in Figure A-1, the complexity of CNN progressively increases from the convolutional layer to the fully connected (FC) layer. This design enables CNN to recognize relatively simple patterns (lines, curves, etc.) before progressing to capture more intricate features (faces, objects, etc.), with the ultimate aim of extracting relevant information for accurate pattern identification. 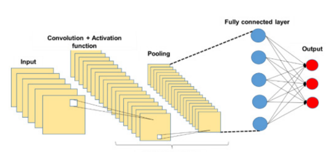 Figure A-1. Structure of basic CNN.

<table>
<tr>
<td></td>
<td>As illustrated in Figure A-2, the convolutional layer is responsible for most computations in the network. This involves extracting local features from an image using a set of learnable filters known as kernels. The behavior of the filter in the convolutional layer is influenced by two main factors: stride and padding. Stride refers to the pixel shift of the filter across the image, while padding aims to preserve information at the corners. In each iteration, a portion of the image is convolved with a filter to generate a dot product of pixels within its receptive field. This process is replicated across the entire image to produce a feature map. The convolution operation is defined as follows:</td>
</tr>
<tr>
<td>2) In section 3.4.2 the equation of the MAPE, MAE and RSME objective function is not presented</td>
<td>We have revised Section 3.4.2, adding detailed explanations of the calculations and the significance of each evaluation metric. These explanations enable readers to better understand the objective function when these evaluation metrics are applied.

3.4.2 Performance Metrics

This study utilized four widely recognized performance measures to assess the ~~model's~~ model's effectiveness in prediction accuracy (Chou and Nguyen, 2023). The measures included mean absolute error (MAE), mean absolute percentage error (MAPE), and root mean square error (RMSE).

MAE represents the mean of absolute errors, calculated as the average of the absolute differences between actual and predicted values. Its advantage lies in its simplicity, which provides a straightforward measure of average prediction error. However, a drawback of MAE is its insensitivity to more significant errors, so it may not effectively highlight differences between models when significant errors are present. It is defined as:

$$MAE = \frac{1}{n}\sum_{i=1}^{n}\left|y_i - \hat{y}_i\right| \quad (5)$$
where n is the number of predictions, y_i is the i^{th} forecasted value, and $\hat{y}_i$ is the corresponding i^{th} actual value.

MAPE quantifies the average absolute error ratio—derived from the differences between actual and forecasted values—to the actual value. It provides a clear metric in percentage terms, facilitating straightforward interpretation across various datasets. However, MAPE's limitation arises from its sensitivity to zero values in the actual data, which can become undefined or impractical to compute, limiting its utility in scenarios involving zero or near-zero actual values. The expression for MAPE is as follows:

$$MAPE = \frac{1}{n}\sum_{i=1}^{n}\left|\frac{y_i - \hat{y}_i}{y_i}\right| \quad (6)$$
where n is the number of predictions, y_i is the i^{th} forecasted value, and $\hat{y}_i$ is the corresponding i^{th} actual value.

RMSE represents the square root of the average squared error between actual and forecasted values and is widely used for its ability to indicate the dispersion of errors. This method captures the magnitude and direction of errors, making it practical for assessing overall prediction accuracy. However, RMSE tends to be more sensitive to outliers and significant errors than MAE due to its squaring of errors during computation. This sensitivity can disproportionately affect its evaluation in datasets with extreme values. The expression for RMSE is as follows:

$$RMSE = \sqrt{\frac{1}{n}\sum_{i=1}^{n}(y_i - \hat{y}_i)^2} \quad (7)$$
where n is the number of predictions, y_i is the i^{th} forecasted value, and $\hat{y}_i$ is the corresponding i^{th} actual value.</td>
</tr>
<tr>
<td>3) Section 3.5 - Chou and Nguyen in 2024 article not present in the bibliography or not mentioned in the correct form</td>
<td>The AEIO algorithm employed in this study was developed in 2024. It has successfully undergone testing on small, average, and large-scale benchmark functions, as well as in optimizing the hyperparameters of AI models. However, since the algorithm is currently under review for publication in a separate journal, we are unable to include it as a reference in this manuscript. We kindly ask for the reviewers' understanding regarding this limitation.
Although we have not added a citation for the AEIO algorithm, we have provided a highly detailed explanation of its usage to ensure that readers can easily understand and apply it, as outlined below.</td>
</tr>
</table>

3.5 Age of Exploration-Inspired Optimizer

This study employs a range of AI models to forecast deep-seated displacement in mountainous regions. To enhance the prediction accuracy of these AI models, the study incorporates a novel metaheuristic optimization algorithm known as the Age of Exploration-Inspired Optimizer (AEIO). Developed by Chou and Nguyen in 2024, this algorithm has demonstrated high effectiveness in fine-tuning the hyperparameters of AI models. This algorithm treats each particle in the search domain as an explorer. The movement of particles toward regions with higher fitness values parallels the exploratory activities of the Age of Exploration, where explorers sought ideal locations for establishing colonies. In this study, each particle represents a set of hyperparameters, with the ultimate goal of the search process being to identify the optimal particle or hyperparameter set that minimizes prediction error for AI models. Figure 8 illustrates the AEIO algorithm.

The strength of the AEIO algorithm lies in its ability to develop specific strategies for particles based on their positions, enabling faster convergence to the optimal point. Using density-based spatial clustering of applications with noise (DBSCAN) for particle clustering, the AEIO determines whether particles are in favorable or unfavorable positions, reminiscent of explorers during the Age of Exploration. The proximity (within clusters) allows explorers to gather information and move toward optimal locations, thereby enhancing their ability to establish new colonies. In contrast, explorers far apart (outside clusters) adopt different strategies, relying on limited peer guidance or general trends in their quest for new territories.

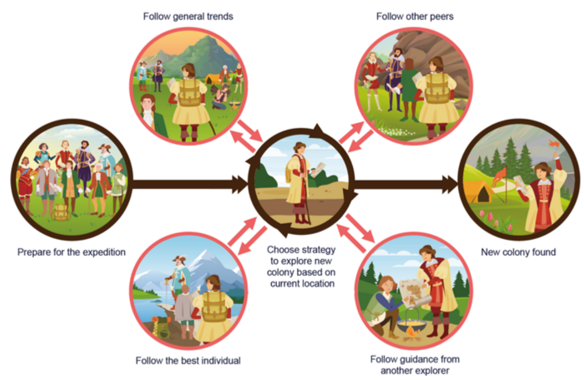

Figure 8. Illustration of Age of Exploration-Inspired Optimizer

In each iteration, explorers forecast their next move. If it promises a better position, they relocate. Otherwise, if the new spot is less favorable for colony establishment, they stay put and await the next iteration. The algorithm employs specific mathematical formulas to calculate the movement step of explorers or particles in the AEIO. The exploratory steps of explorer in the AEIO algorithm will continuously iterate until the stop condition is satisfied.

- **Explorers follow general trends**

The explorer choosing this movement type will calculate the distance from their location $x_{i,d}(t)$ to the center of all other explorers $(Meanvl_d(t))$, then attempt to move towards that central point in the hope of finding a better location with the potential to establish a new colony. The following formula determines the explorer's position after the movement:

$$x_{i,d}(t+1) = x_{i,d}(t) + \alpha * \left(Meanvl_d(t) - x_{i,d}(t)\right) \times rand(0,1) \times R \quad (8)$$

$$Meanvl_d(t) = \frac{x_{1,d}(t) + x_{2,d}(t) + \cdots + x_{n_{Pop},d}(t)}{n_{Pop}} \quad (9)$$

where $d = 1,2, \dots D$; D is the number of dimensions; $i = 1,2, \dots n_{Pop}$; n_{Pop} is the total number of explorers; $t = 1,2, \dots MaxIt$ is the number of iterations; $MaxIt$ is the maximum value of iteration; α is a parameter for adjusting the particle's movement toward the centroid position (usually equals 3). $Meanvl_d(t)$ is the centroid of all particles in dimension d. $rand(0,1)$ is the random number in the range [0,1]. R: a number that equals 1 or 2 depending on the value of $rand(0, 1)$ per the equation. $R = round(1 + rand(0,1) \times 1)$, $x_{i,d}(t)$ is the location of particle i in iteration t, $x_{i,d}(t+1)$ is the location of particle i in iteration $(t+1)$.

- **Explorers follow three other peers**

Explorers employing this movement method will calculate the average position of three randomly selected other explorers $\left(\frac{x_{1,d}(t)+x_{2,d}(t)+x_{3,d}(t)}{3}\right)$ and then move toward this newly calculated average position. The explorer's new position is computed using the following formula:

$$x_{i,d}(t+1) = x_{i,d}(t) + \left(\frac{x_{1,d}(t)+x_{2,d}(t)+x_{3,d}(t)}{3} - x_{i,d}(t)\right) \times rand(0,1) \times R \quad (10)$$

where: $x_{1,d}(t)$, $x_{2,d}(t)$ and $x_{3,d}(t)$ are three random explorers in dimension d at iteration t, $d = 1,2, \dots D$; D is the number of dimensions; $i = 1,2, \dots n_{Pop}$; n_{Pop} is the total number of explorers; $t = 1,2, \dots MaxIt$ is the number of iterations; $MaxIt$ is the maximum value of iteration.

- **Explorers follow the best one**

According to this strategy, the explorer $(x_{i,d}(t))$ will move closer to the position of another explorer currently holding the best position $(Best_d(t))$, as determined by the following formula:

$$x_{i,d}(t+1) = x_{i,d}(t) + \left(Best_d(t) - x_{i,d}(t)\right) \times rand(0,1) \times R \quad (11)$$

where: $Best_d(t)$ represents the position of the particle with the best fitness in dimension d at iteration t, the parameters d and t hold the same significance as defined in Equation 10.

- **Explorers follow guidance from another one**

Explorers in favorable positions with access to information can execute this movement strategy. In this scenario, explorers $(x_{i,d}(t))$ will consult with ~~each other~~ another explorer. The consulted explorer will compare their direction and distance to the best individual, who holds the most favorable position $(Best_d(t))$ and guide the inquirer. This algorithm assumes that the inquirer can be any explorer, i.e., a random explorer $(x_{1,d}(t))$. The following formula describes how to calculate the new position of the explorer following this strategy:

$$x_{i,d}(t+1) = x_{i,d}(t) + \left(Best_d(t) - x_{1,d}(t)\right) \times rand(0,1) \times R \quad (12)$$

where: $x_{1,d}(t)$ is a random explorer in dimension d at iteration t. the parameters d and t hold the same significance as defined in Equation 10.

- **Crowd control mechanism**

To enhance the efficiency of AEIO in transitioning between exploration and exploitation, a mechanism is employed to adjust the parameters of DBSCAN throughout each cycle, according to the following formula:

$$\varepsilon_d = \left(0.1 + \frac{t}{MaxIt}\right) \times \left(Meanvl_d(t) - Best_d(t)\right) \quad (13)$$

$$MinPts = round\left(1 + \frac{t}{MaxIt} \times 10\right) \quad (14)$$

The exploratory steps in the AEIO algorithm begin by classifying positions using the DBSCAN algorithm. Subsequently, the explorers update the crowd control mechanism according to equations (13) and (14), and move according to various strategies defined by equations (8), (10), (11), and (12). This process is conducted iteratively, continuing until the maximum number of iterations is reached.

To fine-tune the hyperparameters of AI models, the AEIO algorithm treats each hyperparameter as a variable. Furthermore, the objective function of the AEIO algorithm seeks to minimize the prediction error of AI models, which is quantified by an evaluation metric (MAPE). Figure 4 presents a flowchart illustrating the process by which the AEIO algorithm aids in fine-tuning hyperparameters for AI models.

Additionally, the AEIO algorithm demonstrated strong optimization capabilities for the hyperparameters of AI models in this study, highlighting its effectiveness.

4) Section 3.5 - EQ. 10 and 11 - The meaning of the Maxit and Mind parameters are not indicated

We acknowledge the error in our initial manuscript, as pointed out by the reviewer's suggestion. We have now added annotations for the parameters d, D, n_{pop}, t, and MaxIt in Equation (10). Additionally, we have clarified that these values hold the same meaning in Equations (11) and (12).

- **Explorers follow three other peers**

Explorers employing this movement method will calculate the average position of three randomly selected other explorers $\left(\frac{x_{1,d}(t)+x_{2,d}(t)+x_{3,d}(t)}{3}\right)$ and then move toward this newly calculated average position. The explorer's new position is computed using the following formula:

$$x_{i,d}(t+1) = x_{i,d}(t) + \left(\frac{x_{1,d}(t)+x_{2,d}(t)+x_{3,d}(t)}{3} - x_{i,d}(t)\right) \times rand(0,1) \times R \quad (10)$$

where: $x_{1,d}(t)$, $x_{2,d}(t)$ and $x_{3,d}(t)$ are three random explorers in dimension d at iteration t, $d = 1,2,\dots D$; D is the number of dimensions; $i = 1,2,\dots n_{Pop}$; n_{Pop} is the total number of explorers; $t = 1,2,\dots MaxIt$ is the number of iterations; $MaxIt$ is the maximum value of iteration.

- **Explorers follow the best one**

According to this strategy, the explorer $(x_{i,d}(t))$ will move closer to the position of another explorer currently holding the best position $(Best_d(t))$, as determined by the following formula:

$$x_{i,d}(t+1) = x_{i,d}(t) + \left(Best_d(t) - x_{i,d}(t)\right) \times rand(0,1) \times R \quad (11)$$

where: $Best_d(t)$ represents the position of the particle with the best fitness in dimension d at iteration t, the parameters d and t hold the same significance as defined in Equation 10.

- **Explorers follow guidance from another one**

Explorers in favorable positions with access to information can execute this movement strategy. In this scenario, explorers $(x_{i,d}(t))$ will consult with ~~each other~~ another explorer. The consulted explorer will

<table>
<tr>
<td></td>
<td>
compare their direction and distance to the best individual, who holds the most favorable position ($Best_d(t)$) and guide the inquirer. This algorithm assumes that the inquirer can be any explorer, i.e., a random explorer ($x_{1,d}(t)$). The following formula describes how to calculate the new position of the explorer following this strategy:

$$x_{i,d}(t+1) = x_{i,d}(t) + \left(Best_d(t) - x_{1,d}(t)\right) \times rand(0,1) \times R \quad (12)$$

where: $x_{1,d}(t)$ is a random explorer in dimension d at iteration t. the parameters d and t hold the same significance as defined in Equation 10.
</td>
</tr>
<tr>
<td>5) Section 3.6.0-In Figure 9, references are indicated to the 18-19-20-21 and 22 equations. But these equations do not exist and the text</td>
<td>
We have revised the equation numbering in this flowchart to ensure consistency with the sequence of equations presented earlier.

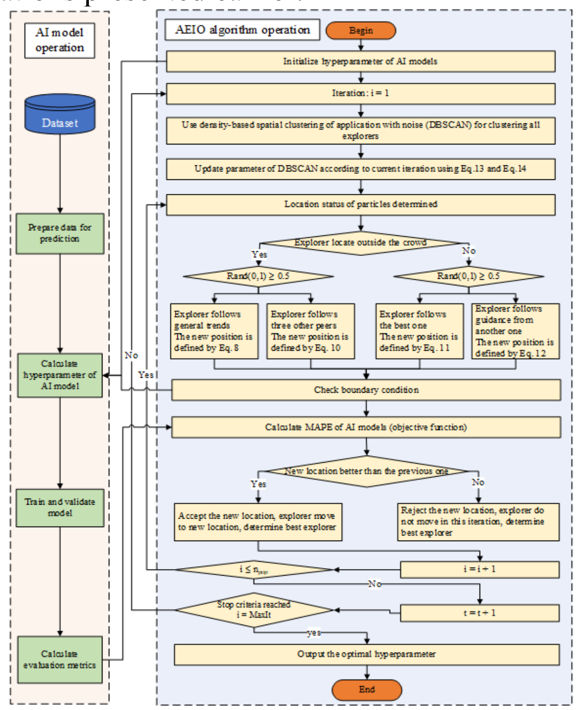

Figure 9. Flowchart of the fine-tuning process of AI models by the AEIO algorithm
</td>
</tr>
<tr>
<td>6) section 3.6.0 in Figure 9 and in the text the optimization stop criterion should be indicated.</td>
<td>
We fully agree with the reviewer's suggestion and have added content to the manuscript to emphasize the stop criterion of the AEIO algorithm.

In each iteration, explorers forecast their next move. If it promises a better position, they relocate. Otherwise, if the new spot is less favorable for colony establishment, they stay put and await the next iteration. The algorithm employs specific mathematical formulas to calculate the movement step of explorers or particles in the AEIO. The exploratory steps of explorer in the AEIO algorithm will continuously iterate until the stop condition is satisfied.

The exploratory steps in the AEIO algorithm begin by classifying positions using the DBSCAN algorithm. Subsequently, the explorers update the crowd control mechanism according to equations (13) and (14), and move according to various strategies defined by equations (8), (10), (11), and (12). This process is conducted iteratively, continuing until the maximum number of iterations is reached.

We have also incorporated the stop criterion into the flowchart of the AEIO algorithm during the fine-tuning of the AI model's hyperparameters.
</td>
</tr>
</table>

	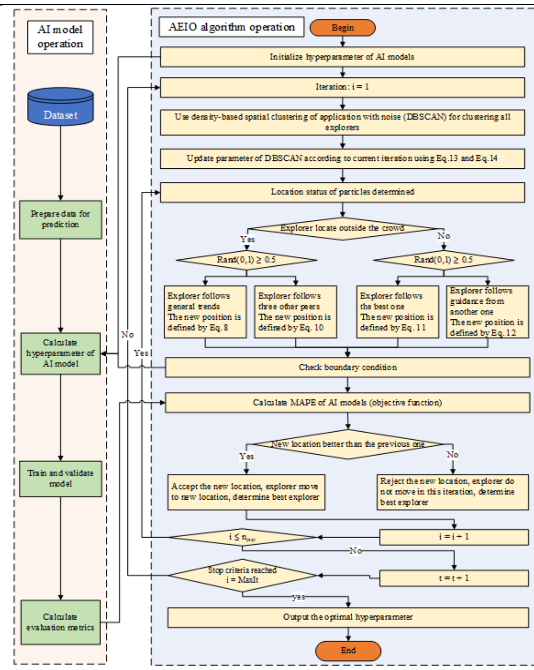 Figure 9. Flowchart of the fine-tuning process of AI models by the AEIO algorithm
7) Section 3.6.2. Figures 12 13 and 14 should be presented together in the same group with the same temporal axis. And an additional figure should be added to the group, with the temporal sequence of the rains	We have revised these figures by merging Figures 12, 13, and 14 into a single figure, presented along a unified timeline. Additionally, the new figure includes rainfall data from significant storms in the region to facilitate easier comparison for the readers. 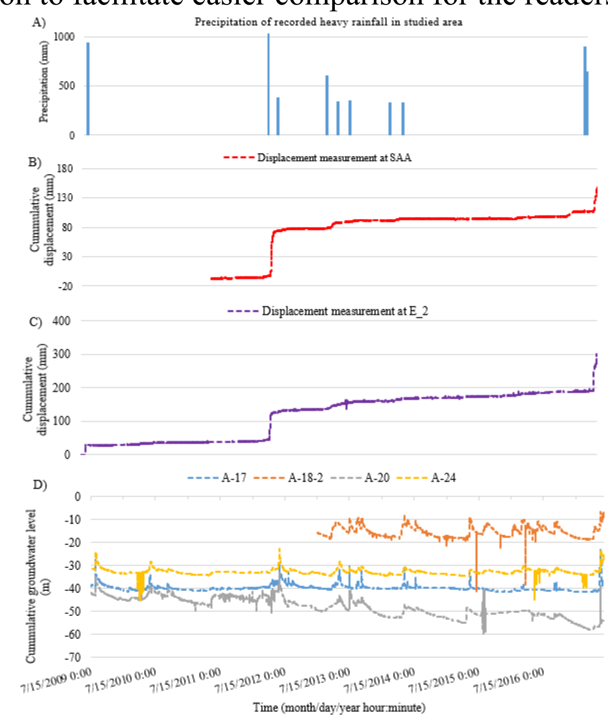 Figure 12. Unified timeline visualization of data in this study. A) Precipitation of recorded heavy rainfall in the studied area; B) Measured displacements from extensometer SAA C) Measured displacements from extensometer E_2; D) Groundwater levels at stations A-17, A-18-2, A-20, and A-24.
8) in Section 4, the comparative result of the deformations observations (shown in figure 14) with	In response to the reviewer's suggestion, we have added a figure that displays the predicted deep-

the comparative predictions of the best model should be graphically presented.	seated displacement of the best machine learning model, the best time-series deep learning model, the best CNN model, and the best hybrid models. This allows readers to compare and assess the predictive capabilities of these models. Figure 10 illustrates the differences between typical AI models' actual and predicted deep-seated displacement. Specifically, Figure 10a compares the performance of single models against the predicted values, while Figure 10b does the same for hybrid models. The chart shows that, hybrid models demonstrate superior predictive capability for deep-seated landslides compared to single models. This is evident from the displacement line of the hybrid models in Figure 10b which closely aligns with the actual deep-seated displacement and significantly outperforms the single models depicted in Figure 10a. 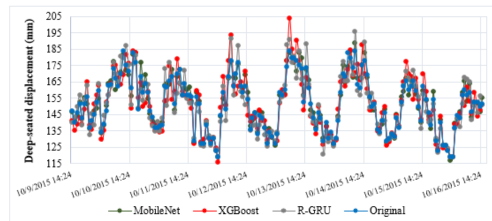 a) Prediction results of deep-seated displacement by single AI models. 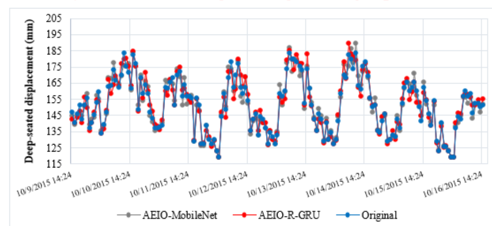 b) Prediction results of deep-seated displacement by AI models optimized using the AEIO algorithm. Figure 10. Graph comparing the real and predicted deep-seated displacement.
9) section 4.2 is too long and should be simplified and synthesized	We fully understand the reviewer's concern regarding the length of Section 4.2. However, it is important to note that much of the length is due to the inclusion of performance result tables for the models, which are essential and cannot be condensed. Additionally, we believe that the explanations and commentary on the models' performance are equally essential. These details not only enhance the manuscript's relevance to readers interested in landslide research but also appeal to those focused on the use of AI models for regression studies. Last but not least, while this section is lengthy, it is organized in a logical structure. As a result, readers will not be distracted by its length; instead, they can easily find information on the specific models they are interested in, corresponding to each subsection within Section 4.2. However, in response to the reviewer's valuable suggestion, we have revisited Section 4.2 and removed redundant content, retaining only the information that is most valuable to the readers.

	660 most suitable machine learning model for predicting deep-seated landslides, exhibiting both high 661 prediction accuracy and a short running time. ~~The following section will compare this model with the best~~ 662 ~~time series deep learning model to select the optimal numerical model for fine-tuning.~~ 664 Similar to the machine learning models, in this section, the time series deep learning models will 665 also be trained with default hyperparameters, as found in research of ~~Chou and Nguyen's research in 2023~~ 666 Chou and Nguyen (2023). The performance results of these models are shown in Table 7. Overall, akin to 679 demonstrates higher prediction accuracy. Therefore, the R-GRU model will be chosen as the best 680 numerical AI model. ~~R-GRU will undergo fine-tuning in the following section using the AEIO algorithm,~~ 681 ~~further enhancing this model's accuracy.~~ 692 displacement of R-GRU before fine-tuning was 7.9%, but this number decreased to only 3.03% after fine- 693 tuning. ~~All other predictions similarly show a decreasing trend.~~ 703 Additionally, Table 9 indicates that predictions from the dataset of the E-2 station consistently 704 outperform those of the SAA station. Specifically, the displacement prediction at the E-2 station is 3.03% 705 and 6.38%, better than the corresponding numbers for the SAA station, which are 3.94% and 7.96%, 706 respectively. This is attributed to the dataset collected by the E-2 station being more comprehensive and 707 gathered over a more extended period than the SAA station (as shown in Table 4). 763 the AEIO algorithm, are presented in Table 14. ~~Compared to models in previous sections,~~ CNN models 764 with optimal hyperparameters ~~obtained in this section exhibit the most minor errors, indicating that these~~ 765 are the most effective models in this study for predicting deep-seated displacement ~~landslide occurrences~~. 771 Figure 10 illustrates the differences between typical AI models' actual and predicted deep-seated 772 displacement. Specifically, Figure 10a compares the performance of single models against the predicted 773 values, while Figure 10b does the same for hybrid models. The chart shows that, hybrid models 774 demonstrate superior predictive capability for deep-seated landslides compared to single models. This is 775 evident from the displacement line of the hybrid models in Figure 10b which closely aligns with the actual 776 deep-seated displacement and significantly outperforms the single models depicted in Figure 10a.